

ORIGINAL ARTICLE

Neuritin Enhances Synaptic Transmission in Medial Prefrontal Cortex in Mice by Increasing $Ca_v3.3$ Surface Expression

Jun-Mei Lu¹, Dong-Dong Liu¹, Zhao-Yang Li¹, Chen Ling² and Yan-Ai Mei¹

¹State Key Laboratory of Medical Neurobiology and School of Life Sciences, Institutes of Brain Science, Fudan University, Shanghai 200433, China and ²State Key Laboratory of Genetic Engineering, School of Life Sciences, Zhongshan Hospital, Fudan University, Shanghai 200032, China

Address correspondence to Chen Ling, State Key Laboratory of Genetic Engineering, School of Life Sciences, Zhongshan Hospital, Fudan University, Shanghai 200032, China. Email: lingchenchina@fudan.edu.cn; Yan-Ai Mei, State Key Laboratory of Medical Neurobiology and School of Life Sciences, Institutes of Brain Science, Fudan University, Shanghai 200433, China. Email: yamei@fudan.edu.cn

Abstract

Neuritin is a neurotrophic factor involved in neural development and synaptic plasticity. However, its role in modulating synaptic transmission remains unclear. Here, we investigated the effects of neuritin on miniature excitatory postsynaptic currents (mEPSCs) and glutamate release in the medial prefrontal cortex (mPFC) in mice. Incubation of mPFC slices with neuritin for 45 min significantly increased mEPSC frequency and glutamate release as measured by high-performance liquid chromatography, which was mimicked by insulin and abrogated by an insulin receptor (IR) inhibitor. Neuritin-induced upregulation of synaptic transmission was correlated with activation of ERK, and inhibition of mitogen-activated protein kinases/extracellular signal-regulated kinases (MEK/ERK) activity attenuated the neuritin-induced increase in mEPSC frequency and glutamate release. T-type calcium channel inhibitors but not the L-type inhibitor abolished the inward calcium current and the effects of neuritin on mEPSC frequency and glutamate release. Western blotting of membrane proteins showed that neuritin promoted surface expression of $Ca_v3.3$ α -subunit, which was also eliminated by inhibition of IR or MEK/ERK activity. The effects of neuritin on mEPSC frequency, glutamate release, and $Ca_v3.3$ α -subunit expression were inhibited by an intracellular protein-transport inhibitor. These results confirm involvement of the IR and ERK signaling pathway, and provide novel insights into the mechanisms of neuritin function in synaptic transmission.

Key words: $Ca_v3.3$, mEPSCs, neuritin, prefrontal cortex, transmitter release

Introduction

Neuritin, also known as candidate plasticity gene 15 (CPG15), was originally isolated during screening for genes induced by kainate-stimulated seizures in rat dentate gyrus and in humans (Nedivi et al. 1993; Naeve et al. 1997). Neuritin was subsequently identified as an important neurotrophin, with multiple roles in neural development, including during synaptic plasticity, synaptic maturation, and dendritic outgrowth

(Cantalops et al. 2000; Javaherian and Cline 2005; Karamoysoyli et al. 2008). Neuritin is a small, highly conserved protein attached to the cell membrane via a glycosylphosphatidylinositol anchor (Nedivi et al. 1993). Although it has been shown to exert non-cell-autonomous functions by binding to receptors (Nedivi et al. 1998; Cantalops et al. 2000), no specific neuritin receptor has yet been identified. Meanwhile, the physiological functions mediated via its receptor and the related intracellular

signals remain unclear. We recently reported that neurtin upregulated the expression of I_A channel Kv4.2 subunits in rat cerebellum granule cells (CGNs) via insulin receptor (IR)-activated mitogen-activated protein kinases/extracellular signal-regulated kinases (MEK/ERK) and Akt/mammalian target of rapamycin (mTOR) signaling pathways (Yao et al. 2012). However, whether the same receptors and signaling pathways occur in other neurons remains to be determined.

Recent investigations of animal cognitive behavior in vivo suggested that neurtin improved synaptic plasticity. Son et al. (2012) reported that loss of neurtin contributed to depressive symptoms caused by stress, and that virus-mediated neurtin expression had antidepressant activity and prevented the atrophy of dendrites and spines caused by chronic unpredictable stress. Similarly, cortical and hippocampal expression of neurtin was shown to be reduced in the brains of Alzheimer's disease patients, and virus-mediated expression of neurtin in the dentate gyrus attenuated learning and memory deficits in an Alzheimer's disease animal model, as determined by the Morris water maze test (Choi et al. 2014). We recently demonstrated that virus-mediated overexpression of neurtin increased the density of dendritic spines, and reversed deficits in novel object associative recognition memory in mice, caused by exposure to extremely low-frequency (50 Hz) electromagnetic fields (Zhao et al. 2015). However, direct evidence for neurtin-mediated modification of synaptic plasticity and synaptic transmission is lacking. Recently, studies have identified that T-type Ca^{2+} channels control Ca^{2+} entry during depolarization near resting potential and facilitated neurotransmitter release (Carbone et al. 2014), whether T-type channels contribute to neurtin-mediated effect on synaptic transmission is also unclear.

Neurtin messenger RNA (mRNA) and protein were first detected in the *Xenopus* spinal cord during development (Hallbook et al. 1991). Neurtin mRNA levels were highest in the brain (Putz et al. 2005), and its expression was upregulated by neuronal activity following chemically induced or electroconvulsive seizures (Nedivi et al. 1993; Naeve et al. 1997; Newton et al. 2003), ischemia and traumatic brain injury (Rickhag et al. 2007; He et al. 2013), and exercise (Hunsberger et al. 2007). A 12% increase in neurtin expression in the rat hippocampus was also observed 1 h after acute electroconvulsive stimulation, and reached a maximal 75% increase after 4 h, suggesting a fast and instantaneous increase in neurtin (Dyrvig et al. 2014). Thus, the nature of the sudden increase in neurtin needs to be established in light of our previous report on neurtin-mediated upregulation of ion-channel proteins at the transcriptional and translation levels (Yao et al. 2012).

In this study, we evaluated the short-term effects of neurtin on synaptic transmission in mouse medial prefrontal cortex (mPFC) slices by recording miniature excitatory postsynaptic currents (mEPSCs) and T-type voltage-gated calcium channel (VGCC) ($I_{T\text{-type VGCC}}$) currents, while simultaneously measuring glutamate release and Ca^{2+} channel protein expression on the membrane. We also determined if the IR and MEK/ERK pathways previously shown to be activated by neurtin in CGNs were also activated in mPFC neurons under these conditions.

Materials and Methods

Experimental Animals

Female C57BL/6 mice (3–4 weeks old) were purchased from Slac Laboratory Animal Company (SLC Co, Ltd.) and bred and maintained at Fudan University. Mice were kept under a 12 h

light/dark cycle and provided with food and water ad libitum. All experiments were performed in accordance with the National Institutes of Health Guidelines for the Care and Use of Laboratory Animals. The experimental protocol was approved by the Committee on the Ethics of Animal Experiments of Fudan University (permit number: 20090614-001).

Acute-Slice Preparation

Adult mice were deeply anesthetized using pentobarbital sodium (50 mg/kg) before decapitation and rapid removal of the entire brain to ice-cold, oxygenated (95% O_2 /5% CO_2) cutting solution (220 mM sucrose, 3 mM KCl, 5 mM $MgCl_2$, 1 mM $CaCl_2$, 1.25 mM NaH_2PO_4 , 26 mM $NaHCO_3$, 10 mM glucose [pH 7.3], and 310–320 mOsm/L). Coronal slices of the prefrontal cortex (bregma 3.6–2.5 mm) were cut at 200 μ m using a vibrating microtome (Dosaka) and incubated in oxygenated (95% O_2 /5% CO_2) artificial cerebral spinal fluid (normal ACSF) (125 mM NaCl, 2.5 mM KCl, 2.5 mM $CaCl_2$, 1.5 mM $MgSO_4$, 1 mM NaH_2PO_4 , 26.2 mM $NaHCO_3$, 11 mM glucose 11 [pH 7.3], 300–310 mOsm/L) for 1 h at 34°C and then stored at room temperature.

High-Performance Liquid Chromatography Detection

Brain slices were reconditioned including ventromedial prefrontal cortex. After incubating in normal ACSF for 1 h at 34°C, brain slices were placed in a 96-well plate with 200 μ L oxygenated (95% O_2 /5% CO_2) ACSF including drugs for 45 min. The ACSF was then collected and frozen at –80°C for glutamate detection by high-performance liquid chromatography (HPLC). Slices were homogenized by Dounce tissue grinder (KEXIN) in iced lysis buffer containing protease inhibitor (Sigma), rotated on ice for 40 min, and centrifuged at 13 800 \times g for 20 min at 4°C. Supernatants were collected to measure total protein levels using a Bicinchoninic acid Protein Assay Kit (Generay). The samples were subjected to reversed-phase HPLC (Thermo Fisher Scientific) with fluorometric detection following precolumn derivatization with o-phthalaldehyde to analyze glutamate concentrations, as described previously (Han et al. 2014). Chromatography was performed on a reversed-phase C-18 column using a pH sodium acetate/methanol gradient. Methionine sulfone was added to each sample as an internal standard. External standards containing 40, 400, or 4000 pmol/20 mL glutamate were run at the beginning and end of every group. The peak heights of glutamate were initially normalized to the methionine sulfone peak and then quantified according to the linear relationship between peak height and the amounts of the corresponding standards. Glutamate concentration determined by HPLC was normalized by total protein level and is expressed as mg/mg protein (Agostini et al. 2011).

Immunohistochemistry

Mice were anesthetized with sodium pentobarbital and perfused transcardially with normal saline (0.9%) and then paraformaldehyde (4%). Brains were postfixed in 4% paraformaldehyde overnight at 4°C and coronal sections (40 μ m) were then cut using a vibratome slicer (Leica) for immunofluorescence analysis. Sections were transferred into 0.5 mL blocking solution (5% bovine serum albumin; 0.5% Triton X-100, and 0.05% sodium azide in phosphate-buffered saline [PBS]) in a multi-well plate, placed on a shaker, and shaken gently at room temperature for 1.5–2 h. The blocking solution was then replaced with the following antibody solutions for 2 days at 4°C: mouse anti- $Ca_v3.1$ (1:50, NeuroMab), mouse anti- $Ca_v3.2$ (1:50, NeuroMab), and rabbit anti- $Ca_v3.3$ (1:100,

Santa Cruz Biotechnology) in 1% bovine serum albumin, 0.5% Triton X-100, and 0.05% sodium azide in PBS. After 2 days, the antibody solution was removed and the sections were washed 3 times with PBST (0.1% Triton X-100 in PBS) for 10 min each, with a final wash for 4–5 h. The sections were incubated with secondary antibody solution (fluorescein isothiocyanate-labeled goat anti-mouse IgG, Cy3-labeled goat anti-rabbit IgG, 1:500) overnight at 4°C. The antibody solution was replaced with PBST and the sections were washed 3 times for 10 min each in PBS. 4',6-Diamidino-2-phenylindole (DAPI) was added to the slices to stain the nucleus. All sections were covered with coverslips using an anti-fade mounting medium, and then observed under a Leica SP2 confocal laser scanning microscope (Leica) with a 40× objective (numerical aperture = 1.30). Immunoreactivity was examined at optimal resolution. Confocal photomicrographs were processed to adjust scaling, brightness, and contrast using LAS AF lite software (Leica).

Golgi Staining

The Rapid Golgi Stain kit (FD Neurotechnologies) was used to analyze dendritic spine morphology as previously described (Zhao et al. 2015). Briefly, acute slices were prepared and incubated in normal ACSF and ACSF containing 150 ng/mL neuritin for 45 min, then transferred to an impregnation solution and stored in the dark for 14 days at room temperature. The slices were then incubated in a sucrose solution at 4°C until they contained no residual water (2–7 days), and then mounted onto gelatin-coated slides and allowed to air dry at room temperature for about 2 days. When they were sufficiently dry, sections were rinsed with distilled water and incubated for 10 min in a silver nitrate solution. The slides were rinsed with distilled water before they were dehydrated in absolute alcohol, cleared with xylene, and covered with non-acidic synthetic balsam and coverslips.

Short hairpin adeno-associated virus construction and injection

Short hairpin (sh)RNA targeting the mouse NRN1 gene and non-targeting control shRNA (shNC) sequences were designed and synthesized by Vigene Biosciences. Four sequences targeting NRN1—i.e., 5'-GCAAGTGTGATGCAGTCTTTAATCCAAGAGATTAAAGACTGCATCACACTTGTGTTTTT-3', 5'-GCTGTTACACATACATAATATTCAAGAGATATTACTGTATGTGTAACAGCTTTTTT-3', 5'-GCAACATC CAAGGCAGCTTATTTCAAGAGAATAAGCTGCCTTGGATGTTGTTTTT-3', and 5'-GCACATACAGTAATACCTGAATTTCAAGAGAATTCAGGTATTACTGTATGTGTTTTT-3'—were constructed in one vector, and adeno-associated virus (AAV) serotype 9 (AAV9) (3.5×10^{11} particles per hemisphere) harboring these sequences were generated. Intracerebroventricular virus injection was performed as previously described, which has been shown to result in robust expression in prefrontal cortical neurons. Briefly, postnatal day 0 pups were injected using an SR-8M stereotaxic manipulator (Narishige Scientific Instrument Lab) to position the syringe (1701RN-33 G; Hamilton Bonaduz) as 0.8–1 mm lateral from the sagittal suture, halfway between lambda and bregma. The needle was inserted to a depth of 3 mm, and up to 2 μ L of virus was slowly injected using a 130 micro-injection pump (KD Scientific) over a 5-min period. The syringe was left in place for an additional 5 min to minimize leakage of the liquid along the injection track. The first injection site was allowed to close before injection of the contralateral hemisphere. AAV transfection efficiency in the mPFC was assessed by western blotting 3–4 weeks after infection (Kim et al. 2014).

Patch-Clamp Recordings

Recordings of slices pre-incubated with neuritin/drugs were carried out at room temperature. Neurons selected for electrophysiological recording exhibited typical characteristics of pyramidal neurons in the II/III layer. Slices were kept fully submerged during recording and continuously perfused (3–4 mL/min) with 95% O₂/5% CO₂-equilibrated ACSF. Recording electrodes were pulled from borosilicate glass on a P-97 4-stage puller (Sutter Instruments) and had a resistance of 3–6 M Ω when filled with internal solution. All recordings were made using a conventional patch-clamp technique with a multiclamp 700B amplifier (Axon Instrument). Data acquisition and analysis were carried out using pClamp 10.2 (Axon Instruments) and/or Origin 8 (Microcal Software) software.

mEPSCs were recorded using voltage-clamp mode in ACSF with added 1 μ M tetrodotoxin (TTX) and 1 μ M bicuculline. Recording pipettes were filled with an internal solution containing 150 mM K-gluconate, 0.4 mM ethylene glycol tetraacetic acid, 10 mM 4-(2-hydroxyethyl)-1-piperazineethanesulfonic acid (HEPES), 2 mM Mg-ATP, 0.1 mM Na₂-GTP, and 8 mM NaCl (pH 7.3, 290 mOsm/L). mEPSCs were analyzed using MiniAnalysis software (Synaptosoft).

T-type calcium channel tail currents were recorded in an extracellular solution composed 105 mM NaCl, 2.5 mM KCl, 2.5 mM CaCl₂, 2 mM MgCl₂, 26.2 mM NaHCO₃, 1 mM NaH₂PO₄, 10 mM glucose, 2 mM CsCl, 5 mM 4-AP, and 15 mM tetraethylammonium (pH 7.4), with 1 μ M TTX and 10 μ M nifedipine added before recording. The internal solution contained 125 mM CsCl, 1 mM MgCl₂, 1 mM CaCl₂, 10 mM HEPES, 10 mM EGTA, 3 mM Mg-ATP, and 0.3 mM Tris-GTP (pH 7.2). The tail current recording protocol was a holding potential of –90 mV for 5 ms and depolarization to –40 mV for 20 ms followed by a holding potential of –90 mV for 5 ms.

Synaptic Membrane-Protein Preparation

Brain slices were prepared at 300 μ m, as described above. Slices were treated with 150 ng/mL neuritin for 45 min at room temperature. Brain slices from each mouse were divided into control and neuritin-incubated groups, with left and right brains from at least 6 mice. Synaptic membrane proteins were prepared as described previously (Kamat et al. 2014). Brain slices were suspended in a 10% (w/v) solution of 0.32 M sucrose-HEPES buffer in a Dounce tissue grinder with protease inhibitor. Suspended tissues were then homogenized by 10 even up-and-down strokes. The homogenate was then centrifuged at 4°C for 10 min at 600×g in a 5424 R centrifuge (Eppendorf). The supernatant was diluted 1:1 with 1.3 M sucrose-HEPES buffer to yield a suspension at a final concentration of 0.8 M sucrose-HEPES. This suspension was centrifuged a further 2 or 3 times at 12 000×g for 15 min at 4°C and the supernatant was discarded each time. The pellet consisting of synaptosomes was suspended in RIPA buffer (Beyotime) (mixed with protease inhibitor and phenylmethylsulfonyl fluoride) and centrifuged at 20 000×g for 30 min. The suspension was reserved and used immediately for protein estimation and western blotting. HEPES-buffer solution consisted of 145 mM NaCl, 5 mM KCl, 2 mM CaCl₂, 1 mM MgCl₂, 5 mM glucose, and 5 mM HEPES, pH 7.4.

Western Blot Analysis

The protocol for western blotting was as follows. Brain slices were lysed in lysis buffer containing 20 mM HEPES, 150 mM NaCl, 0.5% Nonidet P-40, 10% glycerol, 2 mM ethylenediaminetetraacetic acid,

100 μM Na_3VO_4 , 50 mM NaF (pH 7.5), and 1% protease inhibitor for 30 min at 4 °C. After centrifugation at 13 800 $\times g$ for 20 min at 4 °C, the supernatant was mixed with 2 \times sodium dodecyl sulfate loading buffer and boiled for 30 min at 37 °C. Membrane-protein extraction was carried out using a Membrane and Cytosol Protein Extraction Kit (Beyotime), according to the manufacturer's instructions. Proteins were separated by 10% sodium dodecyl sulfate–polyacrylamide gel electrophoresis and transferred to a polyvinylidene difluoride membrane (Millipore) blocked with 10% nonfat milk, and incubated at 4 °C overnight with anti-pERK (1:1000, Cell Signaling Technology), anti-tERK (1:1000, Cell Signaling Technology), anti-Ca ν 3.1 (1:500, NeuroMab), anti-Ca ν 3.2 (1:500, NeuroMab), anti-Ca ν 3.3 (1:200, Santa Cruz), anti-Na-K ATPase (1:1000, Cell Signaling Technology), or anti-GAPDH (1:1000, Beyotime) antibodies. After extensive washing in Tris-buffered saline with 0.3% Tween 20, the membrane was incubated with horseradish peroxidase-conjugated anti-mouse or anti-rabbit IgG (1:5000, KangChen Bio-Tech) for 2 h at room temperature. Protein bands were visualized by chemiluminescence using the SuperSignal West Pico trial kit (Pierce) and detected using a ChemiDoc XRS system (Bio-Rad). Quantity One v.4.6.2 software (Bio-Rad) was used for background subtraction and quantification of immunoblotting data.

Data Analysis

One- or 2-way analysis of variance (ANOVA) followed by Fisher's least significant difference post hoc tests was used for multiple comparisons of electrophysiology, western blot, and HPLC data. Two-sample comparisons were performed using the paired-sample and unpaired Student's t-tests. Data are presented as the mean \pm standard error. Electrophysiological data were collected from at least 4 slices from 4 mice on different days. A value of $P < 0.05$ was considered statistically significant.

Chemicals

Recombinant human neuritin was purchased from PeproTech. Insulin, U0126, nifedipine, NiCl_2 , mibefradil, cycloheximide, and actinomycin-D were purchased from Sigma. TTX and TTA-P2 were purchased from Alomone Labs. Hydroxy-2-naphthalenylmethylphosphonic acid (HNMPA) was purchased from Santa Cruz Biotechnology. Brefeldin A and DL-Threo- β -Benzyloxyaspartic acid (DL-TBOA) were obtained from Selleck. Tetanus toxin was obtained from Calbiochem.

Results

Neuritin Increases mEPSC Frequency and Glutamate Release in mPFC Pyramidal Neurons

We recorded mEPSCs from visually identified pyramidal neurons in mPFC layers II/III from cortex slices using whole-cell voltage clamping. mEPSCs were recorded at a holding potential of -70 mV in the presence of 10 μM bicuculline and 1 μM TTX to inhibit GABA $_A$ -mediated inhibitory postsynaptic currents and spontaneous action-potential generation, respectively. Incubation of mPFC slices with neuritin increased the mEPSC frequency in a concentration- and time-dependent manner (Fig. 1A,B). Data from 241 neurons showed that incubation with neuritin 50 ng/mL for 45 min increased mEPSC frequency by 9.63% compared to the control group (from 1.35 ± 0.08 Hz in control to 1.48 ± 0.09 Hz, respectively, $P > 0.05$). Neuritin concentrations of 100, 150, 200, and 300 ng/mL significantly increased mEPSC frequency by 32.59%

(1.79 ± 0.11 Hz; $P < 0.05$), 40.00% (1.89 ± 0.12 Hz; $P < 0.01$), 44.44% (1.95 ± 0.2 Hz; $P < 0.01$), and 55.56% (2.1 ± 0.25 Hz; $P < 0.001$), respectively (Fig. 1A). However, mEPSC frequency was unaffected by incubation with neuritin 150 ng/mL for 10 min compared with the control group (from 1.32 ± 0.05 Hz in control to 1.61 ± 0.13 Hz, $P > 0.05$). Prolonging the incubation time to 20, 30, 45, and 60 min increased mEPSC frequency by 29.55% (to 1.71 ± 0.13 Hz; $P < 0.05$), 33.33% (to 1.76 ± 0.12 Hz; $P < 0.05$), 49.24% (to 1.97 ± 0.11 Hz; $P < 0.001$), and 80.30% (to 2.38 ± 0.29 Hz; $P < 0.001$), respectively (Fig. 1B), but had no significant effect on mEPSC amplitude (Fig. 1C). Representative cumulative distributions of interevent intervals and amplitudes are shown in Figure 1D.

Changes in mEPSC frequency are thought to be caused by modulation of presynaptic transmission. We, therefore, measured glutamate concentrations in the ACSF by HPLC. Neuritin significantly increased glutamate release by 162.79% compared with the control group (from 0.12 ± 0.02 mg/mg in control vs. 0.32 ± 0.06 mg/mg with neuritin; $P < 0.01$) (Fig. 1E). To exclude the effect of uptake by astrocytes on neuritin-induced glutamate release, we applied the glutamate-uptake inhibitor DL-TBOA to the ACSF. DL-TBOA 10 μM alone increased glutamate release by 177.78% compared with the control group (from 0.12 ± 0.02 mg/mg in the control to 0.33 ± 0.04 mg/mg with DL-TBOA; $P < 0.01$) (Fig. 1E), but neuritin combined with DL-TBOA increased glutamate release by 95.66% and 105.10% as compared with treatment with DL-TBOA and neuritin only, respectively (0.65 ± 0.10 mg/mg with DL-TBOA + neuritin vs. 0.33 ± 0.04 mg/mg with DL-TBOA only and 0.32 ± 0.06 mg/mg with neuritin only; $P < 0.001$) (Fig. 1E), suggesting that the neuritin-induced increase in glutamate concentration in mPFC slices was not due to its effect on glutamate uptake by astrocytes. To determine whether neuritin-induced vesicular release of glutamate, neurons were treated with the vesicular release blocker tetanus toxin (McMahon et al. 1992). Tetanus toxin (10 nM) decreased the neuritin-induced increase in glutamate concentration from 165.00% to -34.23% (from 0.33 ± 0.04 mg/mg with neuritin alone vs. 0.08 ± 0.10 mg/mg with tetanus toxin plus neuritin; $P < 0.01$) (Fig. 1E), suggesting that vesicular release mechanism was involved. Taken together, these data indicated that incubation with 150 ng/mL neuritin for at least 20 min increased mEPSC frequency in pyramidal neurons that was associated with glutamate release, while having no effect on amplitude.

Neuritin Increased mEPSC Frequency and Glutamate Release in Pyramidal Neurons Through Activation of IR-Mediated ERK1/2 Pathway

We previously showed that neuritin increased I_A amplitude and upregulated expression of the K ν 4.2 α -subunit in rat and mouse CGNs through activation of IR-mediated ERK1/2 and Akt/mTOR pathways (Yao et al. 2012). Therefore, in this study we used the IR inhibitor HNMPA and insulin to investigate the role of IR in the effects of neuritin on mEPSC frequency and glutamate release in mouse mPFC neurons. IR inhibition by HNMPA (100 μM) attenuated the effect of neuritin on mEPSC frequency. Co-incubation of mPFC slices with neuritin and HNMPA reduced neuritin-induced upregulation of mEPSC frequency from 64.03% (2.28 ± 0.28 Hz with neuritin alone) to -2.14% (1.37 ± 0.11 Hz with HNMPA plus neuritin; $P < 0.001$) (Fig. 2A), which did not differ from the value obtained by treatment with HNMPA alone. HNMPA also significantly inhibited the neuritin-induced increase in glutamate release from 201.92% (0.51 ± 0.12 mg/mg with neuritin alone) to -32.44%

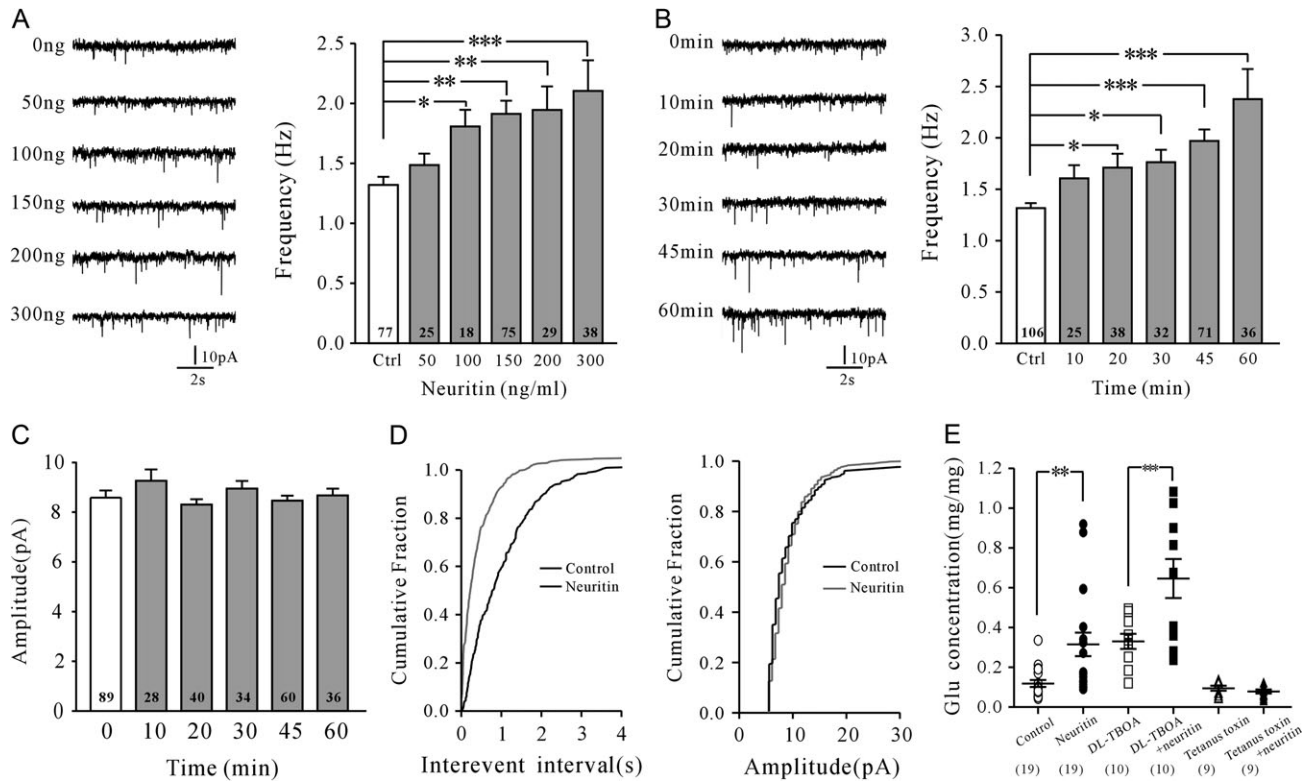


Figure 1. Neuritin significantly increased the frequency of mEPSCs in a concentration- and time-dependent manner. (A) mEPSCs were recorded in control ACSF or ACSF with different concentrations of neuritin. Left panel shows representative recordings; right panel shows frequency of mEPSCs under different concentrations of neuritin. (B) mEPSCs were recorded in control ACSF or ACSF with 150 ng/ml neuritin for different times. (C) mEPSC amplitude was unaffected by neuritin, irrespective of incubation time. (D) Representative cumulative distributions of interevent intervals and amplitudes. (E) Neuritin increased glutamate release with or without DL-TBOA, but tetanus toxin inhibited neuritin-induced glutamate release, as measured by HPLC. Results are shown as means \pm SEM. * $P < 0.05$, ** $P < 0.01$, *** $P < 0.001$ between groups connected by a straight line (one-way ANOVA).

(0.11 ± 0.02 mg/mg with HNMPA plus neuritin; $P < 0.001$) (Fig. 2B). Moreover, insulin mimicked the effects of neuritin on mEPSC frequency and glutamate release. Incubation of mPFC slices with 150 ng/ml insulin increased the mEPSC frequency by 45.65% (from 1.38 ± 0.12 Hz in the control to 2.01 ± 0.15 Hz with insulin; $P < 0.01$) (Fig. 2C) and glutamate release by 90.98% (from 0.28 ± 0.06 mg/mg in the control to 0.54 ± 0.08 mg/mg with insulin; $P < 0.05$) (Fig. 2D).

Yao et al. (2012) previously showed that exposure of CGNs to neuritin markedly induced ERK phosphorylation within 30 min, and increased levels of mTOR at 18 h. We, therefore, examined the effects of neuritin on the ERK signaling pathway in mPFC by measuring the levels of pERK. Phosphorylation of both ERK1 (44 kDa) and ERK2 (42 kDa) were significantly increased by neuritin, as shown by western blotting (Fig. 3A). Treatment of mPFC slices with neuritin (150 ng/ml) for 45 min increased pERK1 and pERK2 levels by $82.3 \pm 28.0\%$ ($P < 0.01$) and $106.1 \pm 34.0\%$, respectively ($P < 0.01$) (Fig. 3A). Consistent with the results of mEPSC frequency, blocking IR with HNMPA reduced neuritin-induced phosphorylation of ERK1 and ERK2 to $1.7 \pm 16.1\%$ ($P < 0.01$) and $18.8 \pm 14.7\%$ ($P < 0.01$), respectively (Fig. 3A). Furthermore, inhibition of the MEK/ERK pathway with U0126 eliminated the effects of neuritin on mEPSC frequency and glutamate release. In the presence of U0126 (10 μ M), the neuritin-induced increase in mEPSC frequency was reduced from 50.36% (2.09 ± 0.17 Hz with neuritin alone) to 5.88% (1.45 ± 0.14 Hz with U0126 plus neuritin; $P < 0.01$) (Fig. 3B). The neuritin-induced increase in glutamate release was also inhibited by U0126, from 381.63%

(0.86 ± 0.18 mg/mg with neuritin alone) to -24.01% (0.18 ± 0.11 mg/mg with U0126 plus neuritin; $P < 0.01$) (Fig. 3C). To confirm whether transcription/translation contributed to the neuritin-mediated increase in glutamate release, mPFC slices were treated with 10 μ M cycloheximide or 10 μ M actinomycin-D to block transcription and translation, respectively. Inhibiting transcription/translation did not abolish the neuritin-induced increase in mEPSC frequency (Fig. 3D). In addition, Golgi staining revealed that spine density in first, second and third order of branches was not increased upon incubation with neuritin for 45 min (Fig. 3E). These data indicated that neuritin activated IR/ERK signaling, which was required for neuritin-mediated enhancement of mEPSC frequency and glutamate release; however, it did not change mPFC neuron spine density within 45 min of treatment.

Neuritin Increased Synaptic Transmission in Pyramidal Neurons in the mPFC via T-Type Calcium Channels

Growing evidence suggests that T-type VGCCs play a key role in controlling neurotransmission near the resting potential and sustaining neurotransmitter release during mild stimulation (Carbone et al. 2014). We, therefore, investigated the association between T-type VGCCs and the neuritin-induced increase in synaptic transmission using specific calcium channel blockers. Treatment of mPFC slices with the T-type VGCC blockers NiCl_2 (100 μ M) or mibefradil (10 μ M) reduced the neuritin-induced increase in mEPSC frequency from 37.81% (1.80 ± 0.10 Hz with neuritin alone) to 5.65% (1.31 ± 0.14 Hz with NiCl_2 plus neuritin;

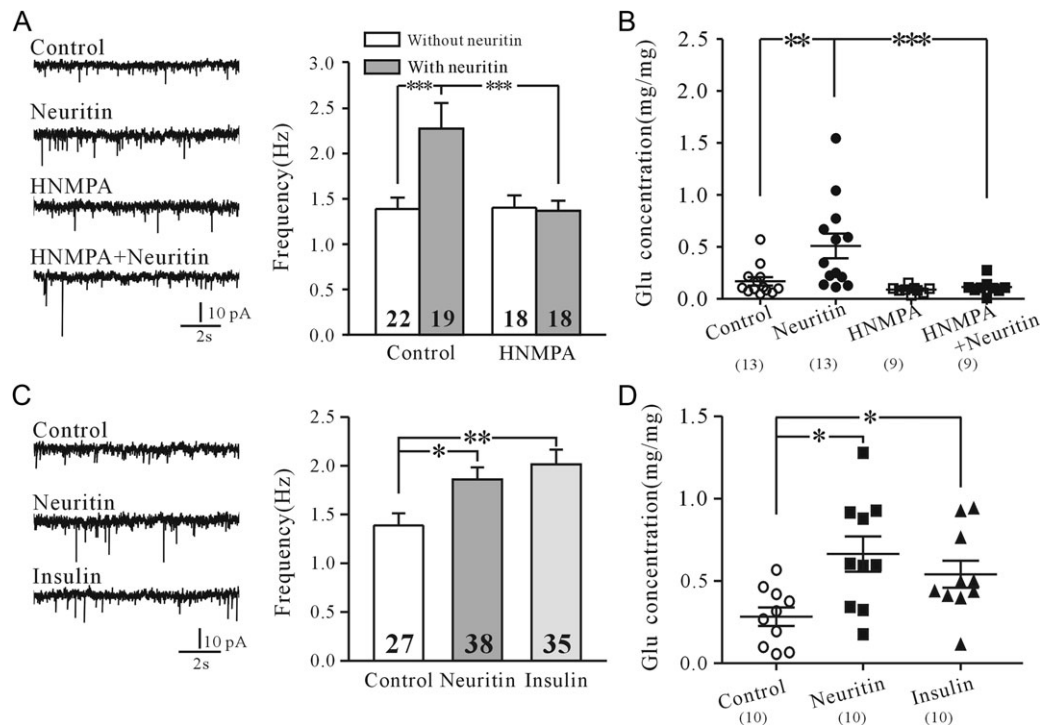


Figure 2. Involvement of IR in neuritin-induced increase in mEPSC frequency and glutamate release. (A) Effects of IR inhibitor HNMPA on neuritin-induced upregulation of mEPSC frequency. (B) Effects of IR inhibitor HNMPA on neuritin-induced increase of glutamate release. (C and D) Insulin mimicked the effects of neuritin on mEPSC frequency and glutamate release. Results are shown as means \pm SEM. * $P < 0.05$, ** $P < 0.01$, *** $P < 0.001$ between groups connected by a straight line (one-way ANOVA).

$P < 0.01$) and -1.19% (from 2.05 ± 0.09 Hz with neuritin alone to 1.66 ± 0.09 Hz with mibefradil plus neuritin; $P < 0.01$), respectively (Fig. 4A,B). A similar result was obtained using the T-type VGCC inhibitor TTA-P2 ($1 \mu\text{M}$), which reduced the neuritin-induced increases in mEPSC frequency and glutamate release from 33.77% (2.02 ± 0.11 Hz with neuritin alone) to -6.21% (1.37 ± 0.07 Hz with TTA-P2 plus neuritin; $P < 0.001$) and from 82.46% (0.32 ± 0.02 mg/mg with neuritin alone) to -16.29% (0.11 ± 0.02 mg/mg with TTA-P2 plus neuritin; $P < 0.001$), respectively (Fig. 4C,D). We also used nifedipine to exclude a potential role of L-type VGCCs and found that the neuritin-enhanced mEPSC frequency and glutamate release were unaffected by nifedipine alone (Fig. 4E,F). Neuritin increased mEPSC frequency by 42.96% (1.93 ± 0.20 Hz; $P < 0.01$) and glutamate release by 175.45% (0.48 ± 0.13 mg/mg; $P < 0.05$) in the presence of $10 \mu\text{M}$ nifedipine (Fig. 4E, F), suggesting that L-type VGCCs do not play a major role in neuritin-mediated effects on mEPSC frequency and glutamate release.

To confirm the role of T-type VGCCs in neuritin-induced enhancement of mEPSC frequency and glutamate release, we observed the effect of neuritin on $I_{T\text{-type VGCC}}$ in pyramidal neurons in mPFC slices directly. We recorded $I_{T\text{-type VGCC}}$ in the presence of TTX ($1 \mu\text{M}$) and nifedipine ($10 \mu\text{M}$), held at -90 mV and simulated at -40 mV for 20 ms. To avoid possible overlap with R-type calcium channels, we measured the tail currents following the end of the depolarizing pulse (Becker et al. 2008; Ekstein et al. 2012). NiCl_2 ($100 \mu\text{M}$), mibefradil ($10 \mu\text{M}$), and TTA-P2 ($1 \mu\text{M}$) significantly inhibited the current by 79.64% , 70.24% , and 81.89% , respectively (from 190.71 ± 9.65 to 38.83 ± 4.36 , 56.76 ± 6.70 , and 37.78 ± 5.72 pA, respectively, $P < 0.001$); incubation with these inhibitors along with neuritin suppressed the current by 74.58% , 62.18% , and 73.14% , respectively (from 190.71 ± 9.65

to 48.48 ± 4.27 , 72.12 ± 14.42 , and 51.22 ± 6.39 pA, respectively, $P < 0.001$). (Fig. 5A), indicating that the recorded current was mainly $I_{T\text{-type VGCC}}$. As expected, the $I_{T\text{-type VGCC}}$ was significantly increased by 27.78% and 28.06% (from 190.71 ± 9.65 to 243.69 ± 17.10 and 244.22 ± 21.50 pA, respectively; $P < 0.05$ and $P < 0.01$, respectively) after incubation of mPFC slices with neuritin and insulin for 45 min (Fig. 5B). Consistent with the previous results for mEPSCs and pERK, the neuritin-induced increase in $I_{T\text{-type VGCC}}$ was eliminated by the IR inhibitor HNMPA and Akt/ERK pathway inhibitor U0126 (Fig. 5C). In the presence of HNMPA, increases in $I_{T\text{-type VGCC}}$ induced by neuritin were reduced from 19.37% to -12.36% (from 260.28 ± 14.93 pA with neuritin to 191.09 ± 16.88 pA with HNMPA plus neuritin; $P < 0.001$). In the presence of U0126, increases in $I_{T\text{-type VGCC}}$ induced by neuritin were reduced from 32.04% to -24.71% (from 245.52 ± 21.08 pA with neuritin to 140.00 ± 12.49 pA with U0126 plus neuritin; $P < 0.001$) (Fig. 5C). However, U0126 alone reduced the amplitude of the Ca^{2+} current, suggesting that blocking Akt/ERK signaling with U0126 inhibits $I_{T\text{-type VGCC}}$ via an unknown pathway, although the difference was not statistically significant relative to the control; it also did not alter the inhibitory effect of U0126 on the neuritin-induced increase in $I_{T\text{-type VGCC}}$. Overall, these data indicated that neuritin increased T-type VGCC activity via the IR/ERK pathway.

Neuritin Increased T-Type VGCC Activity by Promoting $\text{Ca}_v3.3$ Surface Expression

The effect of neuritin on mEPSCs and glutamate release was short-term, and 45 min was not long enough to influence T-type VGCC proteins transcription and translation. We, therefore, suspected that neuritin may promote membrane

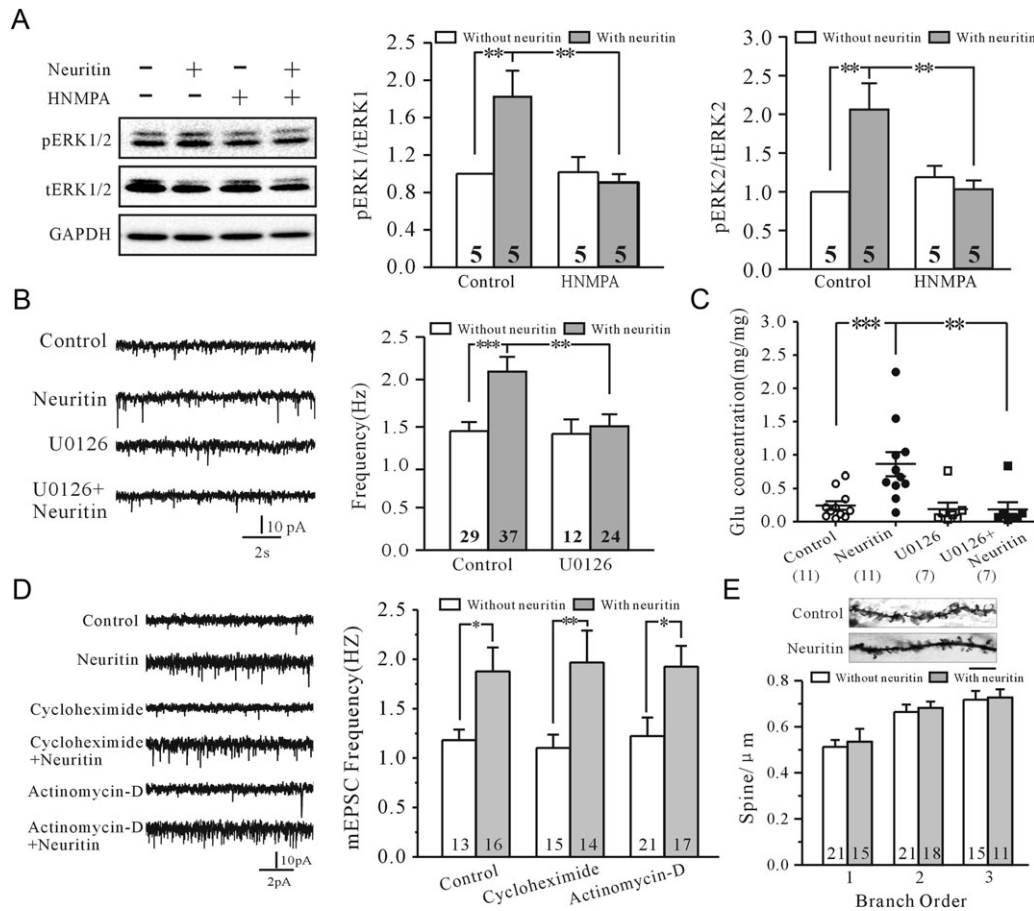


Figure 3. Involvement of IR/ERK pathway in neuritin-induced increase in mEPSC frequency and glutamate release. (A) Representative western blot and bar graph showing effects of neuritin on phosphorylated ERK1/ERK2 levels in the absence and presence of HNMPA. pERK1 and pERK2 levels were normalized by total ERK1 and ERK2 levels. (B) Representative recordings and bar graph showing effects of neuritin on mEPSC frequency in the absence and presence of MEK inhibitor U0126. (C) Effects of U0126 on neuritin-induced increase of glutamate release. (D) Representative recordings and bar graph showing effects of neuritin on mEPSC frequency in the absence and the presence of inhibitors of transcription/translation (cycloheximide and actinomycin-D). (E) Representative Golgi staining and bar graph showing effect of neuritin on spine density. Bar = 10 μ m. Results are shown as means \pm SEM. * $P < 0.05$, ** $P < 0.01$, *** $P < 0.001$ between groups connected by a straight line (one-way ANOVA).

trafficking of T-type VGCC proteins. Using specific antibodies, we confirmed that all 3 α -subunits of T-type VGCCs (Ca_v3.1, Ca_v3.2, and Ca_v3.3) were expressed on mPFC pyramidal neurons (Fig. 6A), consistent with a previous *in situ* hybridization study (Talley et al. 1999). We measured the effect of neuritin on the surface expression of T-type VGCCs in mPFC neurons using a membrane extraction kit. Western blotting results showed that neuritin significantly increased the membrane expression of Ca_v3.3 by $37.39 \pm 4.37\%$ ($P < 0.001$), but had no significant effect on Ca_v3.1 or Ca_v3.2 ($-0.21 \pm 3.35\%$; $P > 0.05$ and $3.52 \pm 11.15\%$; $P > 0.05$, respectively) (Fig. 6B).

These results suggest that Ca_v3.3 membrane expression levels were upregulated by neuritin. We examined Ca_v3 expression at the synaptic membrane to further confirm whether neuritin-induced glutamate release was caused by its effect on T-type VGCC activity. Western blotting indicated that neuritin-enhanced Ca_v3.3 expression at synaptic membranes by $30.19 \pm 8.07\%$ ($P < 0.05$) while increasing and decreasing Ca_v3.1 and Ca_v3.2 expression by $8.34 \pm 4.42\%$ ($P > 0.05$) and $1.84 \pm 10.46\%$ ($P > 0.05$), respectively (Fig. 6C). These results suggested that neuritin may increase Ca_v3.3 surface expression in all neuron membranes, including presynaptic and postsynaptic membranes.

We further investigated the role of the IR/ERK pathway in the neuritin-induced upregulation of Ca_v3.3 using the corresponding inhibitors. Co-incubation of mPFC slices with neuritin and HNMPA abrogated the upregulation of Ca_v3.3 membrane expression from $47.74 \pm 18.09\%$ (neuritin alone) to $6.35 \pm 17.34\%$ (HNMPA plus neuritin; $P < 0.05$), which did not differ from values obtained by treatment with HNMPA alone (Fig. 7A). Similarly, U0126 inhibited the neuritin-induced upregulation of Ca_v3.3 expression from $32.97 \pm 8.46\%$ (neuritin alone) to $2.97 \pm 8.85\%$ (U0126 plus neuritin; $P < 0.05$), which did not differ from the value obtained by treatment with U0126 alone (Fig. 7B).

Brefeldin A is a lactone antibiotic produced by fungi that indirectly inhibits protein-transport from the endoplasmic reticulum to the Golgi apparatus by preventing formation of coat protein I-mediated transport vesicles (Klausner et al. 1992; Dey et al. 2011). We used brefeldin A to determine if the effects of neuritin on the surface expression of Ca_v3.3 and I_{T-type} VGCC and consequent increases in glutamate release and mEPSC frequency were caused by Ca_v3.3 protein trafficking. Incubation with brefeldin A (10 μ M) for 45 min had no significant effect on the surface expression of Ca_v3.3 ($7.08 \pm 11.33\%$ compared with control group; $P > 0.05$), suggesting that there was no effect on

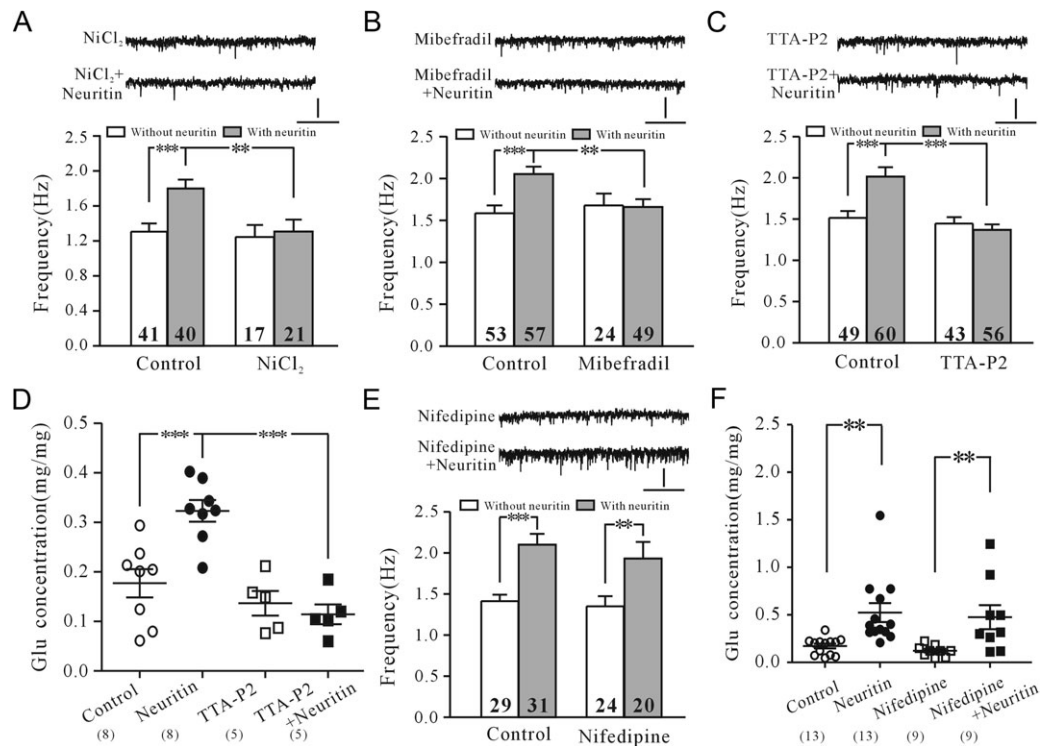


Figure 4. Effects of T-type and L-type VGCC inhibitors on neuritin-induced enhancement of mEPSC frequency and glutamate release. (A–C) Representative recordings and bar graph showing effects of T-type VGCC blockers NiCl₂, mibefradil, and TTA-P2 on neuritin-induced increase in mEPSC frequency. (D) Effect of TTA-P2 on neuritin-induced increase of glutamate release. (E and F) Representative recordings and bar graph showing effects of the L-type VGCC blocker nifedipine on neuritin-induced increases in mEPSC frequency and glutamate release. Results are shown as means \pm SEM. * $P < 0.05$, *** $P < 0.001$ between groups connected by a straight line (one-way ANOVA). Vertical bar = 10 pA, horizontal bar = 2 s.

T-type VGCCs present in the membrane (Fig. 8A). However, co-exposure of brain slices to neuritin and brefeldin A inhibited the increase in membrane expression of T-type VGCC proteins from $31.47 \pm 9.07\%$ to $5.25 \pm 8.25\%$ ($P < 0.01$) (Fig. 8A). Similarly, neuritin failed to increase $I_{T\text{-type VGCC}}$ in the presence of brefeldin A, and the increases in $I_{T\text{-type VGCC}}$ were reduced from 30.25% to -4.04% (from 228.25 ± 11.02 pA with neuritin alone to 171.62 ± 11.44 pA with brefeldin A plus neuritin; respectively; $P < 0.001$) (Fig. 8B). Brefeldin A also reduced the increases in mEPSC frequency induced by neuritin from 27.78% to -0.98% (1.38 ± 0.08 Hz with neuritin alone to 1.01 ± 0.11 Hz with neuritin plus brefeldin A; respectively; $P < 0.01$) (Fig. 8C). HPLC analysis demonstrated that brefeldin A inhibited the neuritin-induced increase in glutamate release from 189.59% to -19.91% (0.75 ± 0.17 mg/mg with neuritin alone to 0.18 ± 0.07 mg/mg with neuritin plus brefeldin A; $P < 0.01$) (Fig. 8D). These results indicate that neuritin increased glutamate release by promoting T-type VGCC trafficking to the membrane.

AAV9-Mediated Neuritin Knockdown Reduces Synaptic Transmission in mPFC Pyramidal Neurons

We investigated whether neuritin is necessary for maintaining synaptic transmission under physiological conditions using AAV9 vectors expressing shRNAs targeting the mouse NRN1 gene. Western blot analysis revealed neuritin expression was reduced by 39.88% relative to shNC infection ($P < 0.05$) (Fig. 9A). The mEPSC frequency was correspondingly reduced by 23.74% (from 1.39 ± 0.10 Hz in the shNC group to 1.06 ± 0.06 Hz in the NRN1 knockdown group; $P < 0.05$) (Fig. 9B). However, mEPSC amplitude did not differ significantly between the 2 groups

(7.14 ± 0.11 pA for NRN1 knockdown and 7.37 ± 0.17 pA for shNC; $P > 0.05$) (Fig. 9B). We also evaluated the effect of NRN1 knockdown on $I_{T\text{-type VGCC}}$ and found that the amplitude of the current was reduced in the NRN1 knockdown group by 38.56% relative to the control (from 130.77 ± 8.48 pA in the shNC group to 80.35 ± 5.77 pA in the NRN1 knockdown group; $P < 0.001$) (Fig. 9C). These results indicate that neuritin is necessary for maintaining synaptic transmission under physiological conditions and that a Ca²⁺-dependent mechanism is involved.

Discussion

We previously demonstrated that neuritin specifically increased the density of I_A in rat CGNs by increasing mRNA and protein expression of Kv4.2 via the IR pathway (Yao et al. 2012). The results of the current study revealed that short-term incubation of cortical neurons with neuritin activated IR signaling, resulting in an upregulation of the Ca_v3.3 subunit of T-type VGCC at the membrane surface, which increased glutamate release and consequently mEPSC frequency. These results confirm that neuritin exerted effects in cortical neurons by activating the same receptors and downstream signaling components as those previously reported in CGNs (Yao et al. 2012), and provide direct evidence for neuritin-mediated modification of synaptic plasticity and synaptic transmission in cortical neurons.

Although previous studies implied that neuritin may function as a ligand (Nedivi et al. 1998; Fujino et al. 2008), few have investigated the receptor responsible for neuritin signal transduction, apart from our previous findings in CGNs (Yao et al. 2012). In the current study, we used pharmacological inhibitors and insulin to demonstrate similar involvement of the

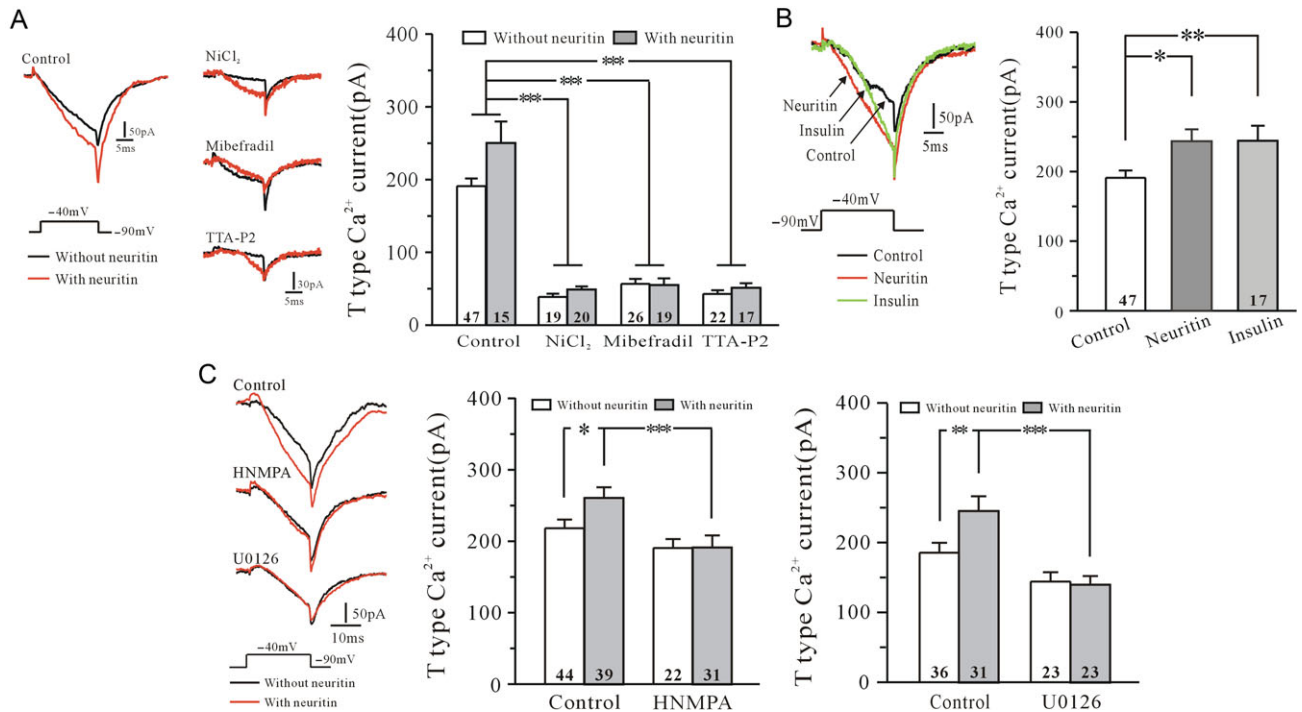


Figure 5. Effect of neuritin on T-type VGCC current ($I_{T\text{-type VGCC}}$) in pyramidal neurons in mPFC. (A) NiCl_2 , mibefradil, and TTA-P2 inhibited $I_{T\text{-type VGCC}}$. $I_{T\text{-type VGCC}}$ was recorded in the presence of TTX and nifedipine, held at -90 mV and stimulated at -40 mV for 20 ms. Tail currents following the end of the depolarizing pulse were measured. Left panel shows representative recordings, right panel shows bar graph of the effects of NiCl_2 , mibefradil, and TTA-P2 on $I_{T\text{-type VGCC}}$ amplitude. (B) Representative recordings and bar graph showing effects of insulin on $I_{T\text{-type VGCC}}$. (C) Representative recordings and bar graph showing effect of HNMPA and U0126 on neuritin-induced increase of $I_{T\text{-type VGCC}}$. Results are shown as means \pm SEM. * $P < 0.05$, ** $P < 0.01$, *** $P < 0.001$ between 2 groups connected by a straight line (Fig. 5A determined by 2-way ANOVA and Fig. 5B,C determined by one-way ANOVA).

IR-mediated ERK pathway in the role of neuritin in synaptic transmission in cortical neurons. Although we did not determine if neuritin bound to the IR receptor directly or indirectly, the results nevertheless revealed that the neuritin/IR/ERK signaling pathway is not specific to CGNs, and may be universal in brain neurons, or at least in cortical neurons. We also noted that blocking MEK/ERK signaling eliminated the effect of neuritin on cortical neurons, suggesting that the mTOR pathway may be unnecessary for neuritin-induced increases in mEPSCs and glutamate release, unlike the effect of neuritin in CGNs that involved activation of both ERK and mTOR signaling pathways for Kv4.2 induction. This difference may be because neuritin upregulates Kv4.2 expression in CGNs at the Akt/mTOR-mediated transcriptional level, but induces $\text{Ca}_v3.3$ expression in cortical neurons at the MEK/ERK-associated posttranslational level.

VGCCs are voltage sensors that convert membrane depolarization into intracellular Ca^{2+} signals; Ca^{2+} influx provides a sensitive and effective means of regulating neurotransmitter release, as a 2-fold change in the presynaptic Ca^{2+} current results in an 8- to 16-fold change in exocytosis (Catterall and Few 2008). In neurons, VGCCs include T-, L-, N-, P/Q-, and R-type Ca^{2+} channels (Catterall and Few 2008; Minor and Fendley 2010), which have all been reported to be involved in spontaneous release events (Missler et al. 2003; Day et al. 2006; Goswami et al. 2012; Jacus et al. 2012; Ermolyuk et al. 2013; Luo et al. 2015) but may be active in different neuron types, different developmental states, and/or different animals. For example, Luo et al. (2015) reported that phenylephrine enhanced mEPSC frequency in layer V/VI pyramidal neurons in the mPFC through interaction with N-type Ca^{2+} channels, while Day et al. (2006)

found that mEPSCs in striatopallidal medium spiny neurons were mediated by the $\text{Ca}_v1.3\alpha1$ subunit of L-type VGCCs. However, increasing evidence suggests that T-type VGCCs are loosely coupled to neurotransmission near the resting potential and sustain neurotransmitter release during mild stimulation, given that these VGCCs are low-voltage activated and control Ca^{2+} entry during depolarization near the resting potential (Cain and Snutch 2010; Carbone et al. 2014). In our study, pharmacological blocking, current recording, and western blotting all suggested that the neuritin-induced increases in mEPSC frequency and glutamate release involved T-type VGCCs. However, a T-type VGCCs blocker alone did not affect the frequency of mEPSCs in cortical neurons under control conditions, and it is possible that a large percentage of T-type calcium channels are tonically inactivated at normal neural resting membrane potentials (Fox et al. 1987; Perez-Reyes 2003; Talavera and Nilius 2006), while only a small proportion of channels remain tonically activated at membrane potentials within the window current (Crunelli et al. 2005). This phenomenon is supported by a previous study (Huang et al. 2011). In addition, it was demonstrated that a $\text{Ca}_v3.2/\text{syntaxin-1A}$ signaling complex was required for T-type channel-mediated, low-threshold exocytosis in MPC9/3L-AH chromaffin cells (Weiss et al. 2012). Further studies are needed to determine whether the neuritin-induced $\text{Ca}_v3.3$ -dependent increase in glutamate release also involves this complex.

T-type/ Ca_v3 Ca^{2+} channels demonstrate molecular diversity as a result of expression and alternative splicing of 3 genes, CACNA1G, CACNA1H, and CACNA1I, encoding the T-type VGCC subunits $\text{Ca}_v3.1/\alpha1\text{G}$, $\text{Ca}_v3.2/\alpha1\text{H}$, and $\text{Ca}_v3.3/\alpha1\text{I}$, respectively (Perez-Reyes E 2003). The biophysical properties, structure-function

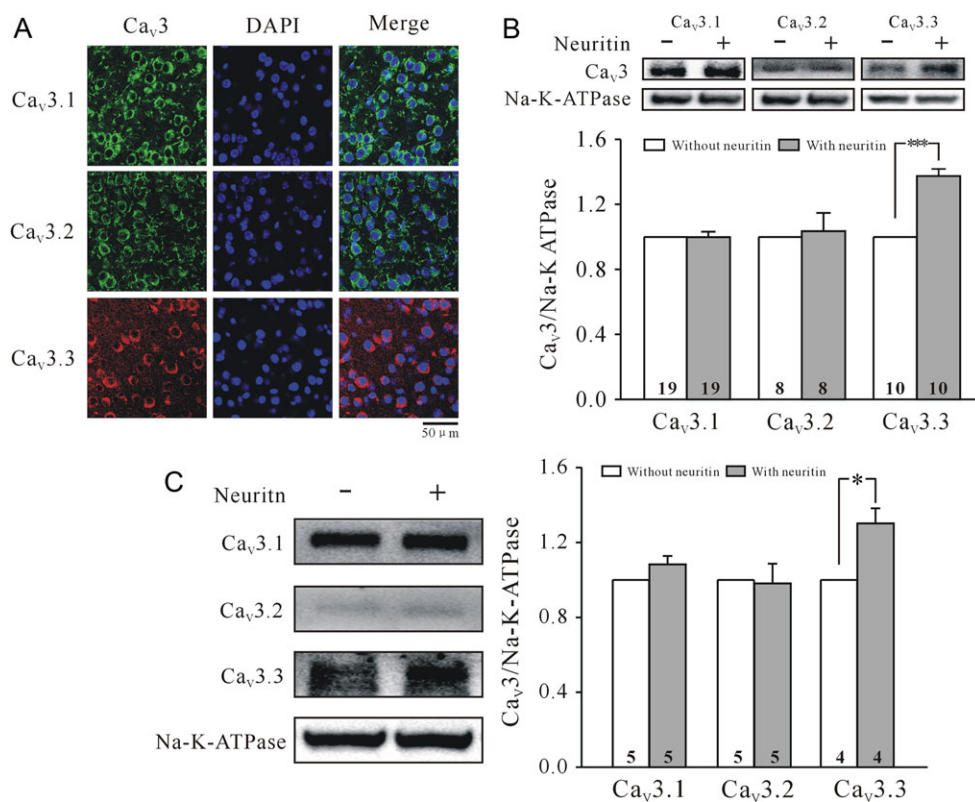


Figure 6. Neuritin-enhanced Ca_v3.3 surface expression on pyramidal neurons in mPFC. (A) Microscopic confocal images showing expression of Ca_v3.1, Ca_v3.2, and Ca_v3.3 α-subunits of T-type VGCCs on pyramidal neurons in mPFC. Bar = 50 μm. (B) Western blot showing effects of neuritin on T-type VGCC surface expression. Na⁺/K⁺-ATPase was used as a loading control. (C) Western blot showing effects of neuritin on T-type VGCC synaptic surface expression. Results are shown as means ± SEM. *P < 0.05, ***P < 0.001 between groups connected by a straight line (paired-sample t-tests).

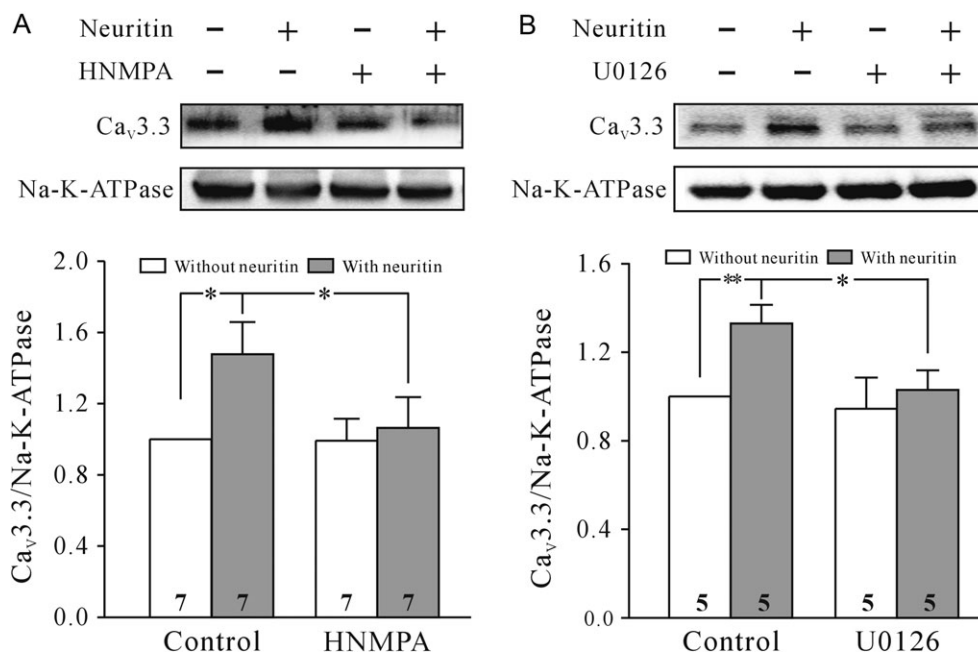


Figure 7. IR/ERK pathway contributed to neuritin-induced enhancement of Ca_v3.3 surface expression on pyramidal neurons in mPFC. (A and B) Western blot showing effects of HNMPA and U0126 on neuritin-induced enhancement of Ca_v3.3 surface expression. Results are shown as means ± SEM. *P < 0.05, **P < 0.01 between groups connected by a straight line (one-way ANOVA).

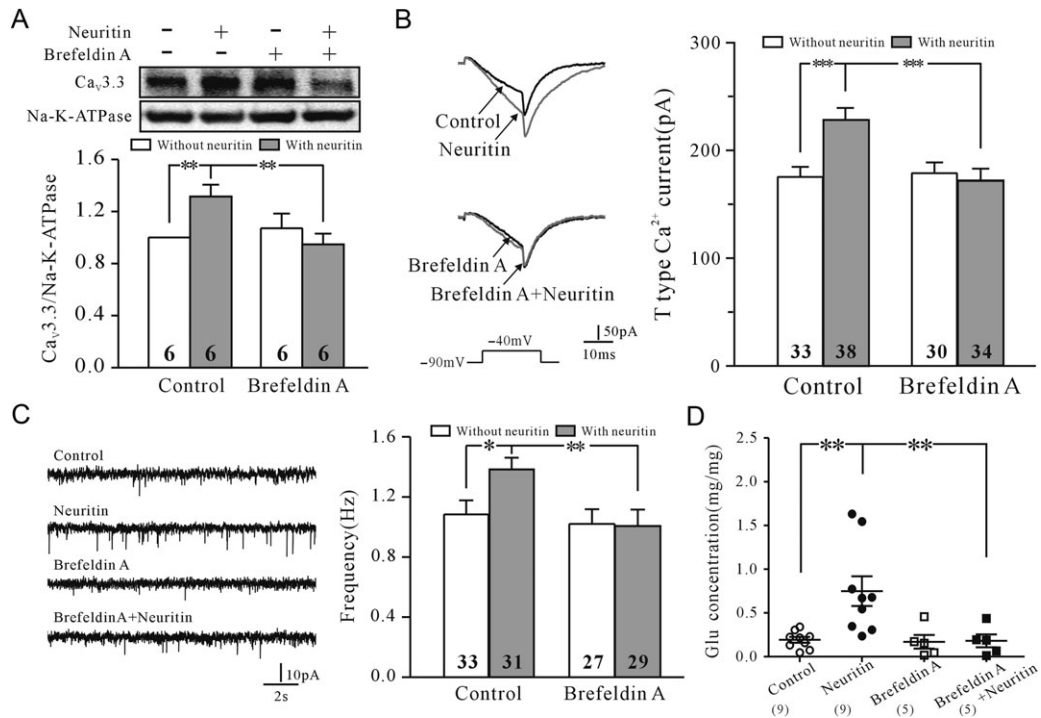


Figure 8. Effects of brefeldin A on neuritin-induced Ca_v3.3 surface expression, I_T-type VGCC amplitude, glutamate release, and mEPSC frequency. (A) Western blot showing effects of brefeldin A on neuritin-induced Ca_v3.3 surface expression. (B) Effect of brefeldin A on neuritin-induced increase in I_T-type VGCC. (C) Representative recordings and bar graph showing abrogation of the effect of neuritin on mEPSCs by brefeldin A. (D) Scatter plot showing effect of brefeldin A on neuritin-induced glutamate release. Results are shown as means ± SEM. *P < 0.05, **P < 0.01, ***P < 0.001 between groups connected by a straight line (one-way ANOVA).

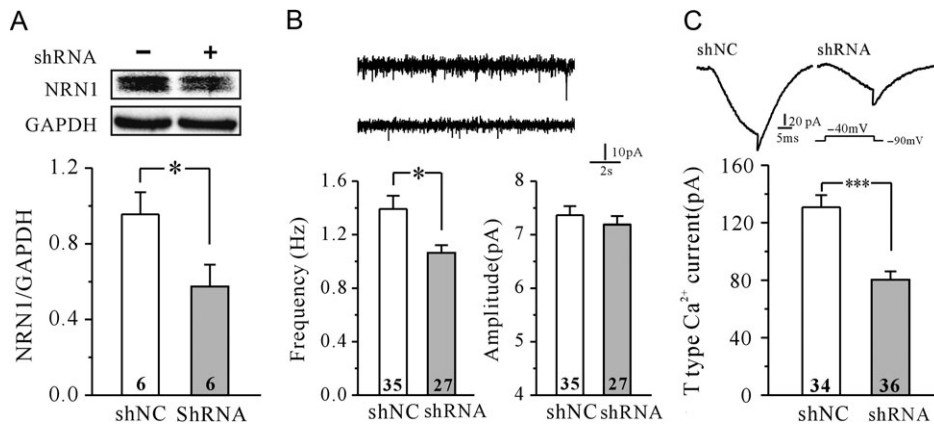


Figure 9. Effect of AAV9-mediated neuritin silencing on synaptic transmission and I_T-type VGCC amplitude in mPFC pyramidal neurons. (A) Western blot showing knockdown of neuritin expression by AAV encoding shRNA targeting the mouse NRN1 gene. (B) Representative recordings and bar graph showing the effect of neuritin knockdown on mEPSC frequency and amplitude. (C) Representative recordings and bar graph showing the effect of neuritin knockdown on I_T-type VGCC amplitude. Results are shown as mean ± SEM. *P < 0.05, ***P < 0.001 between groups connected by a straight line (unpaired Student's t-test).

relationships, and divergent physiological roles of the 3 Ca_v3 channels have been documented (Talavera and Nilius 2006; Baumgart et al. 2008; Huc et al. 2009). In our study, all 3 Ca_v3 subunits were detected in mPFC neurons by immunofluorescence analysis. However, neuritin only enhanced the surface expression of Ca_v3.3, not Ca_v3.1 or Ca_v3.2. T-type VGCCs lack an α-interaction domain to interact with the β-subunit, which usually controls trafficking of other VGCCs to the plasma membrane (Arias et al. 2005). The intracellular loop connecting repeats I and II (I-II loop) of T-type VGCCs thus becomes an important regulator of trafficking, with distinct effects on the 3 channel types (Vitko et al. 2007; Baumgart et al. 2008;

Shcheglovitov et al. 2008). The selective upregulation of Ca_v3.3 by neuritin may be associated with differences in structural properties and trafficking mechanisms among the different Ca_v3 subunits, although further studies are needed to clarify the precise mechanisms involved.

VGCCs subunits can be modulated at multiple levels, including transcription, translation, and trafficking. Long-term upregulation of ion-channel protein expression levels is mainly associated with transcription and translation (Becker et al. 2008; Zhang et al. 2009), while short-term modulation of ion-channel densities may result from rapid mechanisms involving changes in intracellular trafficking of channel proteins (Zhang et al. 2008).

In this study, inhibitors of transcription/translation did not eliminate the increase in mEPSC frequency induced by neuritin, and a 45-min treatment was sufficient to enhance surface expression of Ca_v3.3, suggesting that a short-term modulatory mechanism is responsible. Our speculation that neuritin upregulated Ca_v3.3 surface expression by activation of ERK-mediated trafficking was supported by the effect of the protein-transport inhibitor brefeldin A. Although ERK-mediated protein trafficking is known to play a role in the regulation of T-type VGCC expression, including enhanced surface expression of endogenous Ca_v3.1 channels induced by transient exposure to zinc (Trimarchi et al. 2009; Dey et al. 2011; Mor et al. 2012), there are no known phosphorylation sites for MEK/ERK1/2 on Ca_v3 channels (Huc et al. 2009). In addition, a recent study identified the actin-binding protein Kelch-like 1 as a regulator responsible for enhanced cell surface expression of T-type VGCC proteins (Aromolaran et al. 2010). It is, therefore, important to evaluate the mechanisms whereby ERK upregulates Ca_v3.3 trafficking, and to investigate the possible associations between various components of the ERK signaling cascade and Ca_v3.3 channels following activation of this pathway by neuritin.

The frequency of mEPSCs in somatic neuron recordings is a function of several variables, including the number of synapses, the probability of transmitter release, and the visibility of the synaptic currents. Neuritin was first recognized for its role promoting dendrite/synapse formation (Cantalops et al. 2000; Javaherian and Cline 2005), which has been linked to a subtype of schizophrenia characterized by pervasive cognitive deficits, depression induced by chronic unpredictable stress, and cognitive deficits induced by exposure to extremely low-frequency electromagnetic fields (Son et al. 2012; Zhao et al. 2015; Fatjo-Vilas et al. 2016). The results of the current study provide the first evidence for the positive effects of neuritin on mEPSCs. However, we noted that spine density, length, and diameter or dendrite diameter in mPFC pyramidal neurons were unaltered upon incubation with neuritin for 45 min (data of spine length, diameter, and dendrite diameter not shown), suggesting that changes in the number of synapses are not a key factor in the neuritin-induced increase in mEPSC frequency in this study. A previous study in striatopallidal medium spiny neurons indicated that mEPSC frequency corresponded to a loss of spines and glutamatergic synapses triggered by dysregulation of intrasplinal Ca_v1.3 L-type Ca²⁺ channels (Day et al. 2006). Another study in the developing and adult mouse brain indicated that neuritin stabilized active synapses on dendritic spines in mice, and deletion of neuritin delayed synaptic maturation, and many dendritic spines initially lacked functional synaptic contacts (Fujino et al. 2011). It is also likely that in addition to an increase in T-type channel-mediated low-threshold exocytosis, neuritin-enhanced mEPSC frequency by stabilizing spines and synaptic contacts via upregulation of Ca_v3 channels surface expression, which in turn promoted spontaneous glutamate release in pyramidal neurons.

Neuritin belongs to a subgroup of immediate-early genes implicated in synaptic plasticity, known as effector immediate-early genes (Rickhag et al. 2007). Neuritin expression is rapidly upregulated in ischemia and traumatic brain injury (Rickhag et al. 2007; He et al. 2013) or during exercise (Hunsberger et al. 2007) or electroconvulsive seizures (Nedivi et al. 1993; Naeve et al. 1997; Newton et al. 2003). A significant increase in neuritin expression was also observed in the rat hippocampus 1 h after acute electroconvulsive stimulation (Dyrvig et al. 2014). Our study mimicked the effects of a sudden increase in neuritin level on synaptic transmission and found that a rapid increase

in neuritin-enhanced neurotransmitter release and mEPSC frequency in mPFC neurons, demonstrating a previously unreported role for neuritin in the rapid regulation of cortical neuron activity. This finding suggests that neuritin not only promotes neuronal survival and protects against lesions, but may also rapidly respond to affect neuronal excitability or synaptic activity in the lesioned area via post-transcriptional regulation. We also investigated the effects of neuritin silencing on mEPSC frequency in mPFC neurons and found that neuritin is necessary for maintaining synaptic transmission under physiological conditions, and that this involves a Ca²⁺-dependent mechanism. However, short-term application of neuritin in this study is likely distinct from those regulating the long-term effects of neuritin knockdown, which altered multiple processes, such as neuronal development and synaptic density changes.

The PFC is involved in higher-order brain functions including working memory, attention, behavioral planning, and behavioral flexibility (Goto et al. 2010; Arnsten et al. 2012). The mPFC receives excitatory inputs from basolateral amygdala and ventral hippocampus and has been implicated in recognition memory (Jo et al. 2007; Guirado et al. 2016). Our results revealed that rapid increases in neuritin level in cortical neurons enhanced glutamate release and increased mEPSC frequency, which could affect neuronal excitability or synaptic activity in the mPFC and thereby alter neural network excitability and ultimately, learning and memory. We used acute slices rather than a whole brain for recording mEPSCs, which severed afferent projections from amygdala, ventral hippocampus; thus, we were only able to investigate the effect of neuritin on local excitatory microcircuits (Hempel et al. 2000; Wang et al. 2006). Further learning and memory behavioral tests for ischemia, traumatic brain injury, or electroconvulsive seizures in an animal model are needed to determine the physiological and pathophysiological effects of neuritin on learning and memory involving mPFC neurons.

Supplementary Material

Supplementary data is available at *Cerebral Cortex* online.

Funding

The National Natural Science Foundation of China (nos. NSFC 31370827 and 31428003) and Shanghai Leading Academic Discipline Project (no. B111).

Notes

The authors thank Yuanyuan Ma for assistance in measuring glutamate concentrations by HPLC and Changquan Ling and Yani Zhang at the Second Military Medical University for producing rAAV vectors. Monoclonal antibodies against Ca_v3.1 and Ca_v3.2 were provided by the UC Davis/NINDS/NIMH NeuroMab Facility. *Conflict of Interest*: None declared.

References

Agostini RM, do Nascimento Pinheiro AC, Binda NS, Romano Silva MA, do Nascimento Cordeiro M, Richardson M, Sena Guimaraes AL, Gomez MV. 2011. Phosneutria spider toxins block ischemia-induced glutamate release and neuronal death of cell layers of the retina. *Retina*. 31:1392–1399.

- Arias JM, Murbartian J, Vitko I, Lee JH, Perez-Reyes E. 2005. Transfer of beta subunit regulation from high to low voltage-gated Ca₂₊ channels. *FEBS Lett.* 579:3907–3912.
- Armsten AF, Wang MJ, Paspalas CD. 2012. Neuromodulation of thought: flexibilities and vulnerabilities in prefrontal cortical network synapses. *Neuron.* 76:223–239.
- Aromolaran KA, Benzow KA, Cribbs LL, Koob MD, Piedras-Renteria ES. 2010. T-type current modulation by the actin-binding protein Kelch-like 1. *Am J Physiol Cell Physiol.* 298: C1353–C1362.
- Baumgart JP, Vitko I, Bidaud I, Kondratskyi A, Lory P, Perez-Reyes E. 2008. I-II loop structural determinants in the gating and surface expression of low voltage-activated calcium channels. *PLoS One.* 3:e2976.
- Becker AJ, Pitsch J, Sochivko D, Opitz T, Staniek M, Chen CC, Campbell KP, Schoch S, Yaari Y, Beck H. 2008. Transcriptional upregulation of Cav3.2 mediates epileptogenesis in the pilocarpine model of epilepsy. *J Neurosci.* 28: 13341–13353.
- Cain SM, Snutch TP. 2010. Contributions of T-type calcium channel isoforms to neuronal firing. *Channels (Austin).* 4: 475–482.
- Cantalops I, Haas K, Cline HT. 2000. Postsynaptic CPG15 promotes synaptic maturation and presynaptic axon arbor elaboration in vivo. *Nat Neurosci.* 3:1004–1011.
- Carbone E, Calorio C, Vandael DH. 2014. T-type channel-mediated neurotransmitter release. *Pflugers Arch.* 466:677–687.
- Catterall WA, Few AP. 2008. Calcium channel regulation and presynaptic plasticity. *Neuron.* 59:882–901.
- Choi Y, Lee K, Ryu J, Kim HG, Jeong AY, Woo RS, Lee JH, Hyun JW, Hahn S, Kim JH, et al. 2014. Neuritin attenuates cognitive function impairments in tg2576 mouse model of Alzheimer's disease. *PLoS One.* 9:e104121.
- Crunelli V, Toth TI, Cope DW, Blethyn K, Hughes SW. 2005. The 'window' T-type calcium current in brain dynamics of different behavioural states. *J Physiol.* 562:121–129.
- Day M, Wang Z, Ding J, An X, Ingham CA, Shering AF, Wokosin D, Ilijic E, Sun Z, Sampson AR, et al. 2006. Selective elimination of glutamatergic synapses on striatopallidal neurons in Parkinson disease models. *Nat Neurosci.* 9:251–259.
- Dey D, Shepherd A, Pachuaui J, Martin-Caraballo M. 2011. Leukemia inhibitory factor regulates trafficking of T-type Ca₂₊ channels. *Am J Physiol Cell Physiol.* 300:C576–C587.
- Dyrvig M, Christiansen SH, Woldbye DP, Lichota J. 2014. Temporal gene expression profile after acute electroconvulsive stimulation in the rat. *Gene.* 539:8–14.
- Ekstein D, Benninger F, Daninos M, Pitsch J, van Loo KM, Becker AJ, Yaari Y. 2012. Zinc induces long-term upregulation of T-type calcium current in hippocampal neurons in vivo. *J Physiol.* 590:5895–5905.
- Ermolyuk YS, Alder FG, Surges R, Pavlov IY, Timofeeva Y, Kullmann DM, Volynski KE. 2013. Differential triggering of spontaneous glutamate release by P/Q-, N- and R-type Ca₂₊ channels. *Nat Neurosci.* 16:1754–1763.
- Fatjo-Vilas M, Prats C, Pomarol-Clotet E, Lazaro L, Moreno C, Gonzalez-Ortega I, Lera-Miguel S, Miret S, Munoz MJ, Ibanez I, et al. 2016. Involvement of NRN1 gene in schizophrenia-spectrum and bipolar disorders and its impact on age at onset and cognitive functioning. *World J Biol Psychiatry.* 17: 129–139.
- Fox AP, Nowycky MC, Tsien RW. 1987. Kinetic and pharmacological properties distinguishing three types of calcium currents in chick sensory neurones. *J Physiol.* 394:149–172.
- Fujino T, Leslie JH, Eavri R, Chen JL, Lin WC, Flanders GH, Borok E, Horvath TL, Nedivi E. 2011. CPG15 regulates synapse stability in the developing and adult brain. *Genes Dev.* 25: 2674–2685.
- Fujino T, Wu Z, Lin WC, Phillips MA, Nedivi E. 2008. cpg15 and cpg15-2 constitute a family of activity-regulated ligands expressed differentially in the nervous system to promote neurite growth and neuronal survival. *J Comp Neurol.* 507: 1831–1845.
- Goswami SP, Bucurenciu I, Jonas P. 2012. Miniature IPSCs in hippocampal granule cells are triggered by voltage-gated Ca₂₊ channels via microdomain coupling. *J Neurosci.* 32: 14294–14304.
- Goto Y, Yang CR, Otani S. 2010. Functional and dysfunctional synaptic plasticity in prefrontal cortex: roles in psychiatric disorders. *Biol Psychiatry.* 67:199–207.
- Guirado R, Umemori J, Sipila P, Castren E. 2016. Evidence for competition for target innervation in the medial prefrontal cortex. *Cereb Cortex.* 26:1287–1294.
- Hallbook F, Ibanez CF, Persson H. 1991. Evolutionary studies of the nerve growth factor family reveal a novel member abundantly expressed in *Xenopus* ovary. *Neuron.* 6:845–858.
- Han M, Xiao X, Yang Y, Huang RY, Cao H, Zhao ZQ, Zhang YQ. 2014. SIP30 is required for neuropathic pain-evoked aversion in rats. *J Neurosci.* 34:346–355.
- He Y, Yang G, Wang Y, Ren Y, He X, Zhang X, Fei Z. 2013. Expression of candidate plasticity-related gene 15 is increased following traumatic brain injury. *Neurol Res.* 35:174–180.
- Hempel CM, Hartman KH, Wang XJ, Turrigiano GG, Nelson SB. 2000. Multiple forms of short-term plasticity at excitatory synapses in rat medial prefrontal cortex. *J Neurophysiol.* 83: 3031–3041.
- Huang Z, Lujan R, Kadurin I, Uebele VN, Renger JJ, Dolphin AC, Shah MM. 2011. Presynaptic HCN1 channels regulate Cav3.2 activity and neurotransmission at select cortical synapses. *Nat Neurosci.* 14:478–486.
- Huc S, Monteil A, Bidaud I, Barbara G, Chemin J, Lory P. 2009. Regulation of T-type calcium channels: signalling pathways and functional implications. *Biochim Biophys Acta.* 1793: 947–952.
- Hunsberger JG, Newton SS, Bennett AH, Duman CH, Russell DS, Salton SR, Duman RS. 2007. Antidepressant actions of the exercise-regulated gene VGF. *Nat Med.* 13:1476–1482.
- Jacus MO, Uebele VN, Renger JJ, Todorovic SM. 2012. Presynaptic Cav3.2 channels regulate excitatory neurotransmission in nociceptive dorsal horn neurons. *J Neurosci.* 32: 9374–9382.
- Javaherian A, Cline HT. 2005. Coordinated motor neuron axon growth and neuromuscular synaptogenesis are promoted by CPG15 in vivo. *Neuron.* 45:505–512.
- Jo YS, Park EH, Kim IH, Park SK, Kim H, Kim HT, Choi JS. 2007. The medial prefrontal cortex is involved in spatial memory retrieval under partial-cue conditions. *J Neurosci.* 27: 13567–13578.
- Kamat PK, Kalani A, Tyagi N. 2014. Method and validation of synaptosomal preparation for isolation of synaptic membrane proteins from rat brain. *MethodsX.* 1:102–107.
- Karamoysoyli E, Burnand RC, Tomlinson DR, Gardiner NJ. 2008. Neuritin mediates nerve growth factor-induced axonal regeneration and is deficient in experimental diabetic neuropathy. *Diabetes.* 57:181–189.
- Kim JY, Grunke SD, Levites Y, Golde TE, Jankowsky JL. 2014. Intracerebroventricular viral injection of the neonatal

- mouse brain for persistent and widespread neuronal transduction. *J Vis Exp*. 51863. doi:10.3791/51863.
- Klausner RD, Donaldson JG, Lippincott-Schwartz J. 1992. Brefeldin A: insights into the control of membrane traffic and organelle structure. *J Cell Biol*. 116:1071–1080.
- Luo F, Li SH, Tang H, Deng WK, Zhang Y, Liu Y. 2015. Phenylephrine enhances glutamate release in the medial prefrontal cortex through interaction with N-type Ca²⁺ channels and release machinery. *J Neurochem*. 132:38–50.
- McMahon HT, Foran P, Dolly JO, Verhage M, Wiegant VM, Nicholls DG. 1992. Tetanus toxin and botulinum toxins type A and B inhibit glutamate, gamma-aminobutyric acid, aspartate, and met-enkephalin release from synaptosomes. Clues to the locus of action. *J Biol Chem*. 267:21338–21343.
- Minor DL Jr, Findeisen F. 2010. Progress in the structural understanding of voltage-gated calcium channel (Ca_v) function and modulation. *Channels (Austin)*. 4:459–474.
- Missler M, Zhang W, Rohlmann A, Kattenstroth G, Hammer RE, Gottmann K, Sudhof TC. 2003. Alpha-neurexins couple Ca²⁺ channels to synaptic vesicle exocytosis. *Nature*. 423:939–948.
- Mor M, Beharier O, Levy S, Kahn J, Dror S, Blumenthal D, Gheber LA, Peretz A, Katz A, Moran A, et al. 2012. ZnT-1 enhances the activity and surface expression of T-type calcium channels through activation of Ras-ERK signaling. *Am J Physiol Cell Physiol*. 303:C192–C203.
- Naeve GS, Ramakrishnan M, Kramer R, Hevroni D, Citri Y, Theill LE. 1997. Neuritin: A gene induced by neural activity and neurotrophins that promotes neurogenesis. *Proc Natl Acad Sci U S A*. 94:2648–2653.
- Nedivi E, Hevroni D, Naot D, Israeli D, Citri Y. 1993. Numerous candidate plasticity-related genes revealed by differential cDNA cloning. *Nature*. 363:718–722.
- Nedivi E, Wu GY, Cline HT. 1998. Promotion of dendritic growth by CPG15, an activity-induced signaling molecule. *Science*. 281:1863–1866.
- Newton SS, Collier EF, Hunsberger J, Adams D, Terwilliger R, Selvanayagam E, Duman RS. 2003. Gene profile of electroconvulsive seizures: induction of neurotrophic and angiogenic factors. *J Neurosci*. 23:10841–10851.
- Perez-Reyes E. 2003. Molecular physiology of low-voltage-activated t-type calcium channels. *Physiol Rev*. 83:117–161.
- Putz U, Harwell C, Nedivi E. 2005. Soluble CPG15 expressed during early development rescues cortical progenitors from apoptosis. *Nat Neurosci*. 8:322–331.
- Rickhag M, Teilum M, Wieloch T. 2007. Rapid and long-term induction of effector immediate early genes (BDNF, Neuritin and Arc) in peri-infarct cortex and dentate gyrus after ischemic injury in rat brain. *Brain Res*. 1151:203–210.
- Shcheglovitov A, Vitko I, Bidaud I, Baumgart JP, Navarro-Gonzalez MF, Grayson TH, Lory P, Hill CE, Perez-Reyes E. 2008. Alternative splicing within the I-II loop controls surface expression of T-type Ca_v3.1 calcium channels. *FEBS Lett*. 582:3765–3770.
- Son H, Banasr M, Choi M, Chae SY, Licznarski P, Lee B, Voleti B, Li N, Lepack A, Fournier NM, et al. 2012. Neuritin produces antidepressant actions and blocks the neuronal and behavioral deficits caused by chronic stress. *Proc Natl Acad Sci U S A*. 109:11378–11383.
- Talavera K, Nilius B. 2006. Biophysics and structure-function relationship of T-type Ca²⁺ channels. *Cell Calcium*. 40:97–114.
- Talley EM, Cribbs LL, Lee JH, Daud A, Perez-Reyes E, Bayliss DA. 1999. Differential distribution of three members of a gene family encoding low voltage-activated (T-type) calcium channels. *J Neurosci*. 19:1895–1911.
- Trimarchi T, Pachuau J, Shepherd A, Dey D, Martin-Caraballo M. 2009. CNTF-evoked activation of JAK and ERK mediates the functional expression of T-type Ca²⁺ channels in chicken nodose neurons. *J Neurochem*. 108:246–259.
- Vitko I, Bidaud I, Arias JM, Mezghrani A, Lory P, Perez-Reyes E. 2007. The I-II loop controls plasma membrane expression and gating of Ca_v3.2 T-type Ca²⁺ channels: a paradigm for childhood absence epilepsy mutations. *J Neurosci*. 27:322–330.
- Wang Y, Markram H, Goodman PH, Berger TK, Ma J, Goldman-Rakic PS. 2006. Heterogeneity in the pyramidal network of the medial prefrontal cortex. *Nat Neurosci*. 9:534–542.
- Weiss N, Hameed S, Fernandez-Fernandez JM, Fablet K, Karmazinova M, Poillot C, Proft J, Chen L, Bidaud I, Monteil A, et al. 2012. A Ca_v3.2/syntaxin-1A signaling complex controls T-type channel activity and low-threshold exocytosis. *J Biol Chem*. 287:2810–2818.
- Yao JJ, Gao XF, Chow CW, Zhan XQ, Hu CL, Mei YA. 2012. Neuritin activates insulin receptor pathway to up-regulate Kv4.2-mediated transient outward K⁺ current in rat cerebellar granule neurons. *J Biol Chem*. 287:41534–41545.
- Zhang C, Bosch MA, Rick EA, Kelly MJ, Ronnekleiv OK. 2009. 17Beta-estradiol regulation of T-type calcium channels in gonadotropin-releasing hormone neurons. *J Neurosci*. 29:10552–10562.
- Zhang Y, Helm JS, Senatore A, Spafford JD, Kaczmarek LK, Jonas EA. 2008. PKC-induced intracellular trafficking of Ca_v2 precedes its rapid recruitment to the plasma membrane. *J Neurosci*. 28:2601–2612.
- Zhao QR, Lu JM, Yao JJ, Zhang ZY, Ling C, Mei YA. 2015. Neuritin reverses deficits in murine novel object associative recognition memory caused by exposure to extremely low-frequency (50 Hz) electromagnetic fields. *Sci Rep*. 5:11768.